Fast Plane Wave 2-D Vector Flow Imaging Using Transverse Oscillation and Directional Beamforming

Jensen, Jonas; Villagómez Hoyos, Carlos Armando; Stuart, Matthias Bo; Ewertsen, Caroline; Nielsen, Michael Bachamnn; Jensen, Jørgen Arendt

Published in:
IEEE Transactions on Ultrasonics, Ferroelectrics and Frequency Control

Link to article, DOI:
10.1109/TUFFC.2017.2693403

Publication date:
2017

Document Version
Peer reviewed version

Fast Plane Wave 2-D Vector Flow Imaging Using Transverse Oscillation and Directional Beamforming

Jonas Jensen[1], Carlos Armando Villagómez Hoyos[1], Matthias Bo Stuart[1], Caroline Ewertsen[2], Michael Bachmann Nielsen[2], and Jørgen Arendt Jensen[1]

[1]Center for Fast Ultrasound Imaging, Department of Electrical Engineering, Technical University of Denmark, DK-2800 Lyngby, Denmark
[2]Department of Radiology, Copenhagen University Hospital, DK-2100 Copenhagen, Denmark

***Abstract*—Several techniques can estimate the 2-D velocity vector in ultrasound. Directional beamforming (DB) estimates blood flow velocities with a higher precision and accuracy than transverse oscillation (TO), but at the cost of a high beamforming load when estimating the flow angle. In this paper, it is proposed to use TO to estimate an initial flow angle, which is then refined in a DB step. Velocity magnitude is estimated along the flow direction using cross-correlation. It is shown that the suggested TO-DB method can improve the performance of velocity estimates compared to TO, and with a beamforming load, which is 4.6 times larger than for TO and seven times smaller than for conventional DB. Steered plane wave transmissions are employed for high frame rate imaging, and parabolic flow with a peak velocity of 0.5 m/s is simulated in straight vessels at beam-to-flow angles from 45° to 90°. The TO-DB method estimates the angle with a bias and standard deviation (SD) less than 2°, and the SD of the velocity magnitude is less than 2%. When using only TO, the SD of the angle ranges from 2° to 17° and for the velocity magnitude up to 7%. Bias of the velocity magnitude is within 2% for TO and slightly larger but within 4% for TO-DB. The same trends are observed in measurements although with a slightly larger bias. Simulations of realistic flow in a carotid bifurcation model provide visualization of complex flow, and the spread of velocity magnitude estimates is 7.1 cm/s for TO-DB, while it is 11.8 cm/s using only TO. However, velocities for TO-DB are underestimated at peak systole as indicated by a regression value of 0.97 for TO and 0.85 for TO-DB. An *in vivo* scanning of the carotid bifurcation is used for vector velocity estimations using TO and TO-DB. The SD of the velocity profile over a cardiac cycle is 4.2% for TO and 3.2% for TO-DB.**

I. Introduction

Ultrasound blood flow estimation is of diagnostic value in investigating hemodynamics in the human cardiovascular system. Conventional color flow mapping uses focused emissions in line-by-line imaging, where each line is acquired sequentially from received echoes of several consecutive pulses. It limits the frame rate significantly, when a large color box and large imaging depth are desired, especially when using duplex imaging. The frame rate can drop to 10-15 Hz, and it is impossible to identify rapid temporal changes in the blood flow. Full flow dynamics of both fast and slow flow are also lost, because of the limited observation time along each focusing direction.

Alternative imaging methods such as synthetic aperture imaging (SA) using either spherical or plane waves have been proposed to increase the frame rate and improve image quality [1], [2]. An image of the entire insonified region is created for each emission resulting in a low-resolution image (LRI). By using a few broad insonifications, the low-resolution images can be summed to form a high-resolution image (HRI). The methods require parallel acquisition systems, but enable continuous data in the entire image.

Conventional ultrasound systems are limited to estimation of axial flow velocities only along the ultrasound beam. Several methods have been proposed to estimate the 2-D velocity vector without the need for angle correction, e.g., speckle tracking [3], multibeam methods [4], transverse oscillation (TO) [5]–[7], directional beamforming (DB) [8] and color Doppler-derived vector flow mapping [9], [10]. The 2-D vector flow techniques enable estimation of the true blood velocity in complex vessel geometries and for complex flow phenomena, where the flow angle is not constant. The techniques have also been combined with SA [11], [12] and later with plane waves [2], [13]–[15] for high-frame-rate imaging. More recently, plane wave imaging has been combined with the multibeam method [16]–[19] and transverse oscillation [20].

The TO method estimates the velocity vector by introducing a lateral oscillation in the ultrasound field. Only two lines are beamformed for each estimation point, and the estimators are computationally inexpensive [21]. The precision of the velocity estimates is around 5-10 % with decreased performance for smaller beam-to-flow angles [22]. For the DB approach, lines are focused along the direction of the flow. The velocity magnitude can be estimated with high accuracy and precision using a cross-correlation estimator, due to the high signal correlation along the directional lines. It has also been shown that the standard deviation of the velocity estimates can be reduced by a factor of two, when using DB rather than TO [22]. However, the direction of the blood flow needs to be known in advance for DB. Automatic approaches for angle estimation have been proposed and use either the normalized correlation function (NCF) [23], or velocities estimated on the LRIs to numerically triangulate the flow angle [24]. The number of calculations for these conventional angle estimators is, however, very high because signals have to be beamformed in a 360° polar grid and cross-correlated at every angle and for each estimation point. Lines are usually beamformed at every 5° covering a total of 180° [23], which gives 36 directional lines for every estimation point in each frame.

There is, thus, a tradeoff between performance and beamforming load for the TO and DB methods. In this paper, it is proposed to combine the methods by using TO to automatically estimate an initial flow angle, which is then refined by a NCF DB step. The velocity magnitude is estimated along the refined flow direction as in DB. The method is presented as TO-DB. The objectives are to obtain velocity estimates with an improved performance compared to TO and to have a beamforming load, which is between TO and conventional NCF DB. The concept and first measurements were presented in preliminary versions of the method as published in conference proceedings [25], [26]. This paper expands the theory, and a parameter study of simulated parabolic flow in straight vessel phantoms is performed to reveal the ideal performance of the estimator. Realistic flow derived from computational fluid dynamics (CFD) is simulated in a carotid bifurcation model and included to study the performance of the method for complex flow patterns, which are similar to those obtained *in vivo*. Furthermore, two different echo-canceling filters are applied on an *in vivo* data set to investigate the influence of selecting an appropriate echo-canceling filter.

In the next section, the method for plane wave flow imaging is explained. It is validated using simulations and flow rig measurements, and the methods are described in Section III. The results are presented in Section IV, and the paper is concluded with an example of an *in vivo* scan of the carotid bifurcation of a healthy volunteer.

II. Method for Plane Wave Flow Imaging

This section presents the proposed method for plane wave flow imaging. The principle of plane wave emissions for fast imaging is explained, and the method for vector flow estimation is presented: first, TO estimators are used to find an initial flow angle, and then three directional lines are beamformed around the TO angle to improve the angle estimate. Velocity magnitude is estimated along a fourth line beamformed in the refined flow direction using a cross-correlation estimator. An illustration of the principle is shown in Fig. 1, where three directional lines are beamformed around the initial TO angle estimate.

A. Plane Wave Imaging

High-frame-rate imaging can be obtained by emitting a few plane waves at different steering angles from a linear array transducer. Using the principle of SA imaging [11], a LRI is created for each emission, and a number of LRIs are combined to form an HRI. An HRI has an improved image quality and sensitivity compared to individual LRIs [1], [27], and this principle is used for both flow and B-mode imaging in this paper. Similar to how LRI and HRI can be constructed, low-resolution lines (LRL) and high-resolution lines (HRL) can be beamformed in any desired direction within the insonified region.

B. Transverse Oscillation

A transverse oscillation can be introduced in the pulse-echo field in addition to the conventional axial oscillation, so that

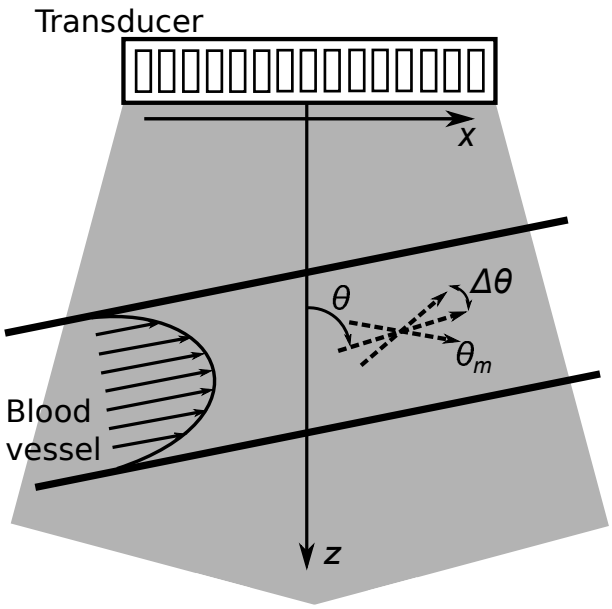

Fig. 1. Plane wave emissions from a linear array transducer are used to insonify flow in a straight vessel. Directional lines are beamformed at angles θ_m around the initial TO angle estimate θ at a single velocity estimation point.

the received signals become sensitive to both an axial and lateral motion in the field. The TO field is usually created in the receive beamforming by changing the apodization function to contain two separate peaks. A lateral oscillation can also be generated in the Fourier domain, known as k-space, to provide better control over the lateral oscillation wavelength. The method was introduced in [28], [29] and is performed in the Fourier domain by filtering the beamformed image in the lateral dimension and only select k-space components around a desired lateral oscillation frequency. The original approach applied a 2-D phase-based block matching estimator for tissue motion estimation, while a fourth order estimator will be used for blood flow estimation in this paper.

The Fourier filtration process is illustrated in Fig. 2. Beamformed data for an HRI has a k-space as illustrated in Fig. 2 (top). An oscillation in the axial direction is centered at the pulse center frequency, while there is no oscillation laterally. A filter $G(f_z, f_x)$ consisting of Gaussian windows centered around a desired TO frequency f_{0x},

$$G(f_z, f_x) = \exp\left(-2(\pi\sigma_x(f_x - f_{0x}))^2\right) + \exp\left(-2(\pi\sigma_x(f_x + f_{0x}))^2\right), \quad (1)$$

where σ_x is the width of the Gaussian window and f_x is the lateral oscillation frequency, is illustrated in Fig. 2 (middle). A multiplication of the filter and the Fourier transformed image gives the TO image in Fig. 2 (bottom). The image has been filtered in the lateral dimension, while the axial dimension is untouched. Any values of the parameters f_{0x} and σ_x can in principle be chosen, but it should be ensured that only k-space components containing energy from flow and not only noise are chosen. By having an effective $F\#$ that is relatively small, energy is retained for larger f_x.

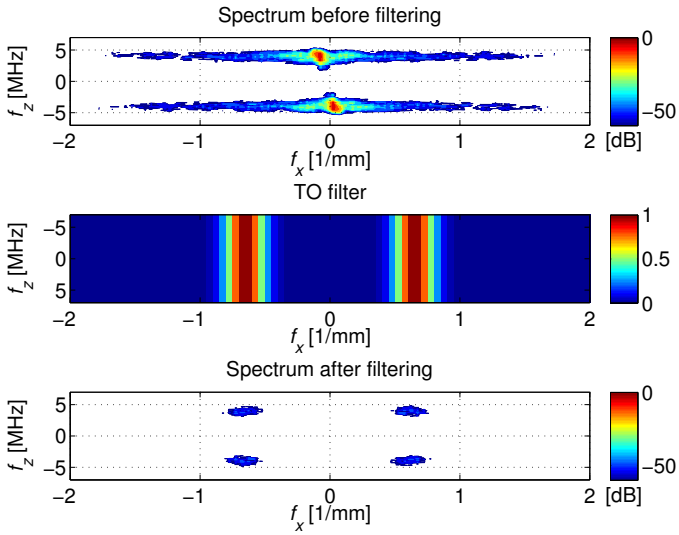

Fig. 2. The 2-D Fourier spectrum of a beamformed RF image is shown in the top figure. The spectrum of the TO filter $G(f_z, f_x)$ is shown in the middle, and the spectrum of beamformed RF image after applying the TO filter is shown in the lower figure. The resulting RF image contains transverse oscillations with a mean lateral frequency according to the desired oscillation frequency of the TO filter.

The directional information of the flow is preserved by keeping only one quadrant of the Fourier spectrum. This avoids applying the Hilbert transform on the TO image or having a spatial quadrature between two beamformed signals [21]. A standard fourth order autocorrelation estimator for the transverse velocity component v_x is employed as proposed in [30]. For the axial velocity component v_z, a cross-correlation estimator is employed [31].

The flow angle is found at each estimation point from:

$$\theta = \arctan\left(v_x, v_z\right) \tag{2}$$

using the estimated v_x and v_z.

C. Directional Beamforming

The initial angle estimate from (2) is used to construct a directional line, where points are focused at

$$\vec{r}_p(k) = \left(\Delta r \cdot k \cdot \sin\theta + x_{st}, \Delta r \cdot k \cdot \cos\theta + z_{st}\right), \tag{3}$$

where Δr is the spatial sampling interval, k is the sample index, and (x_{st}, z_{st}) is the velocity estimation point. Beamforming for the points $\vec{r}_p(k)$ gives a directionally focused signal $y_d(k)$. The pulse repetition period is T_{prf} and the number of LRIs per HRI is N_t, thus, cross-correlating signals from two HRIs gives

$$\begin{aligned} R_{12}(l) &= \frac{1}{N_k+1}\sum_{k=-N_k/2}^{N_k/2} y_d^{(n)}(k) y_d^{(n+N_t)}(k+l) \\ &= \frac{1}{N_k+1}\sum_{k=-N_k/2}^{N_k/2} y_d^{(n)}(k) y_d^{(n)}(k+l-k_s) \\ &= R_{11}(l-k_s) \end{aligned}$$

where $y_d^{(n)}(k)$ is the directional signal focused after emission n, N_k is the number of samples in $y_d(k)$, and $R_{11}(l-k_s)$ is the shifted autocorrelation of $y_d^{(n)}(k)$. A global maximum is attained at $l = k_s$.

Lines can also be beamformed at other angles θ_m, and beamforming three directional signals at $\theta_m \in \{\theta - \Delta\theta, \theta, \theta + \Delta\theta\}$ yield correlation functions $R_{12}(l, \theta_m)$. They are used to calculate the normalized cross-correlation estimate

$$R_{12n}\left(\theta_m\right) = \left(\frac{\max\left(R_{12}(l,\theta_m)\right)}{P_{12}(\theta_m)}\right), \tag{4}$$

which gives the maximum normalized cross-correlation as a function of the angle, and

$$P_{12}(\theta_m) = \sqrt{\sum_k y_d^{(n)}(k,\theta_m)^2 \cdot \sum_k y_d^{(n+N_t)}(k,\theta_m)^2} \tag{5}$$

represents the power of the signals. Using three angles for directional beamforming, $R_{12n}\left(\theta_m\right)$ has three values. The angle estimate, θ_d, is found as the angle yielding the largest correlation

$$\theta_d = \arg\max_{\theta_m}\left\{R_{12n}\left(\theta_m\right)\right\}. \tag{6}$$

If $R_{12}\left(\theta_m\right)$ has its peak value at the center angle, the accuracy of the angle estimate can be improved using a parabolic interpolation [32]

$$\hat{\theta} = \theta_d - \frac{R_{12n}(\theta+\Delta\theta) - R_{12n}(\theta-\Delta\theta)}{2\left(R_{12n}(\theta+\Delta\theta) - 2R_{12n}(\theta) + R_{12n}(\theta-\Delta\theta)\right)}\Delta\theta, \tag{7}$$

where $\Delta\theta$ is the angle span between the three directional lines. Three angle estimates - one for each line - are sufficient to perform a parabolic interpolation, where the correlation values are weights in the interpolation. If the peak value of $R_{12}\left(\theta_m\right)$ is not at the center angle, the corresponding angle θ_m is chosen. $\Delta\theta$ can be selected as a fixed angle span or depend on the estimated TO angle as presented in this paper and explained in Section III.

The angle estimate $\hat{\theta}$ from (7) is then used to beamform a fourth directional line at this angle. The velocity magnitude can be found from the lag of the maximum cross-correlation $R_{12}(l, \hat{\theta})$

$$l_{max} = \arg\max_l R_{12}(l, \hat{\theta}), \tag{8}$$

which corresponds to the velocity magnitude

$$|v| = \frac{l_{max}\Delta r}{T_{prf} N_t}. \tag{9}$$

The accuracy of the velocity estimates can be enhanced by making an interpolation around the maximum lag l_{max} using an equation similar to (7).

D. Beamforming Load

The beamforming load for the TO, TO-DB and DB methods are very different as will be shown here. Considering a single velocity estimation point, the TO method requires two beamformed lines: one axial containing N_z samples and one lateral containing N_x samples, in total

$$N_{TO} = N_z + N_x. \tag{10}$$

For TO-DB, four directional lines are beamformed additionally, each containing N_x samples

$$N_{TO-DB} = N_z + 5 \cdot N_x. \tag{11}$$

For a conventional NCF DB estimator the number of directional lines are usually 36 [23]:

$$N_{DB} = 36 \cdot N_x. \tag{12}$$

Typical values are $N_z = 30$ and $N_x = 250$ for a line length of 1.5λ axially and 12.5λ laterally/directionally as will be used in this paper. The ratio between the TO-DB and TO method is

$$\frac{N_{TO-DB}}{N_{TO}} = \frac{N_z + 5 \cdot N_x}{N_z + N_x} = \frac{30 + 5 \cdot 250}{30 + 250} = 4.6 \tag{13}$$

and between the DB and TO-DB method

$$\frac{N_{DB}}{N_{TO-DB}} = \frac{36 \cdot N_x}{N_z + 5 \cdot N_x} = \frac{36 \cdot 250}{30 + 5 \cdot 250} = 7 \tag{14}$$

Thus, the beamforming load for TO-DB is 4.6 times larger than for TO, but seven times smaller than for conventional NCF DB.

III. Methods for Simulations and Experiments

This section describes the simulation method and the implementation on the experimental scanner SARUS [33] for flow rig measurements and *in vivo* scanning.

A 192-element 0.6λ-pitch transducer is employed, and a duplex sequence is constructed to interweave both flow and B-mode emissions. Three steered flow emissions are emitted at a pulse repetition frequency f_{prf}, and then a B-mode emission is transmitted. It results in an effective pulse repetition frequency, $f_{prf,eff} = f_{prf}/4$, for flow estimation. To construct a full B-mode image, 21 emissions are used, which are selected based on the optimization in [34]. Transducer and acquisition parameters are listed in Table I. A short excitation pulse (1.5-cycle sinusoid) is used for the flow emissions, since the precision of the cross-correlation estimator used for DB is proportional to the bandwidth of the system [32]. Conversely, the precision of the TO phase-shift estimator is inversely proportional to the system bandwidth. This requirement is met by convolving the beamformed signals used for TO estimation with a 4-cycle sinusoid at wavelength λ to achieve narrow-band signals. Similar signals could have been received, if the excitation pulse had a pulse length of 5-6 cycles, which is often used for a phase-shift estimator.

Delay-and-sum beamforming are performed using the Beamformation Toolbox III [35] and processing parameters are listed in Table II. Dynamic receive apodization with an $F\#$ of 0.8 is applied, which is within the angular response of the transducer elements [34]. At each velocity estimation point, an axial and lateral line are used to estimate v_z and v_x with the TO method. For the TO-DB angle refinement, three directional lines are beamformed at each estimation point: one at the TO angle θ and at $\pm\Delta\theta$. The selected angle span $\Delta\theta$ depends on the estimated TO angle:

$$\begin{aligned} \Delta\theta = 2^\circ \text{ for } |\theta| \geq 80^\circ, \\ \Delta\theta = 5^\circ \text{ for } 50^\circ \leq |\theta| < 80^\circ, \\ \Delta\theta = 10^\circ \text{ for } |\theta| < 50^\circ. \end{aligned} \tag{15}$$

TABLE I
Transducer and Acquisition Parameters.

Parameter	Value
Number of elements	192
Transducer center frequency f_0	4.1 MHz
Element pitch	0.2 mm (0.6λ)
Element height	6 mm
Elevation focus	38 mm
Cycles in emitted pulse	1.5 (flow) and 1 (B-mode)
Transmit apodization	Tukey (weight 0.5)
Pulse repetition frequency f_{prf}	10 kHz
Max steering angle	15° (flow) and 20°(B-mode)
Number of plane waves	3 (flow) and 21 (B-mode)

TABLE II
Processing Parameters.

Parameter	TO	TO-DB
Receive apodization	Tukey (weight 0.5)	Tukey (weight 0.5)
Receive F-number	0.8	0.8
Sampling interval dr	$\lambda/20$	$\lambda/20$
Desired lateral wavelength	1.53 mm	-
TO window size	1.5 mm	-
Number of HRI/estimate	32	32
Line length	-	12.5λ

The selection of $\Delta\theta$ is based on the standard deviation (SD) of the TO angle estimate θ. As it covers 68 % of the estimates around θ, it is 68 % confident that the flow angle is within $\Delta\theta$, when considering a normal distribution. This is further explained in Section IV-A1.

Each velocity estimate is obtained by correlating 32 HRIs. For constant flow, 10 non-consecutive estimates are used to calculate the mean and SD of the velocity estimates at each estimation point.

Echo-canceling of beamformed data is performed with a Hoeks filter [36] for simulated and measured flow in a flow rig. For *in vivo* data, an energy-based filter with manual threshold is used [37], [38]. The energy-based cut-off filter is used instead of a conventional frequency cut-off filter to better separate the blood signal from the tissue signal of the moving vessel wall. This is important for transverse flow estimation, because the velocity spectra of blood and tissue will overlap more as shown in Fig. 3. The energy-based filter uses energy or amplitude characteristics of blood and tissue, and tissue components are attenuated by limiting the amplitude of the tissue velocity spectrum to a cut-off threshold A_c. Thus, energy of the narrow-band tissue signal, $\int G'(\omega_t)d\omega$, is overpowered by the energy of a more broad-band blood signal $\int G(\omega_b)d\omega$. Here, the threshold A_c is manually determined after calculating the energy-levels of tissue and blood, and the value depends on the particular scan.

A. Simulations

Simulations of channel RF data are performed using the Field IIpro program [39]–[41]. Constant parabolic flow is simulated inside a straight rigid-wall vessel with a radius of 6 mm and centered at a depth of 20 mm. The vessel is rotated to the angle θ, and the peak velocity of the flow

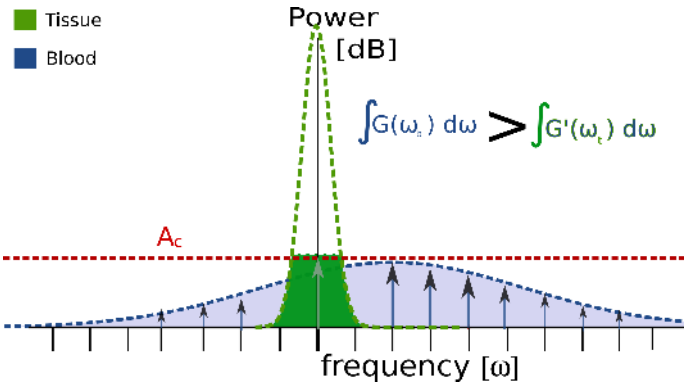

Fig. 3. Velocity spectra for the tissue signal (green curve) and blood signal (blue curve). The energy-based echo-canceling filter limits the velocity spectrum of tissue to an amplitude cut-off A_c. The energy of tissue signal (green area) is overpowered by the energy of the blood signal (blue area).

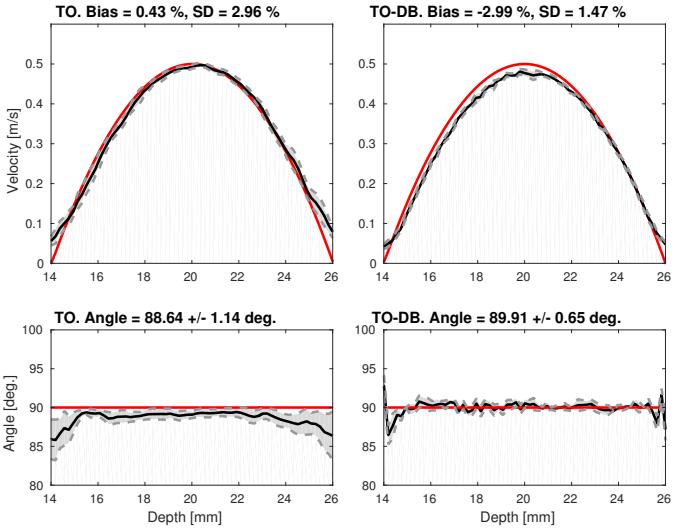

Fig. 4. Simulated velocity profiles for a straight vessel phantom at a 90° beam-to-flow-angle. Velocity magnitude (top) and angles (bottom) for TO (left) and TO-DB (right). Mean estimates are shown in black with ±1 SD and true profiles are in red.

is 0.5 m/s. Approximately 10 point scatterers are simulated per resolution cell randomly distributed and with amplitudes generated from a Gaussian distribution. The influence of noise on the performance of the TO estimator is also investigated in a separate simulation study for a beam-to-flow angle of 90°. White noise is added to the received element RF signals before beamforming to obtain signal-to-noise ratios (SNR) corresponding to specified levels for the HRI. No vessel wall is simulated and echo-canceling is disabled for the SNR investigation.

A carotid bifurcation model is also employed for investigation of more complex flow conditions in a realistic vascular geometry. A computational fluid dynamics (CFD) dataset provided by Swillens et al. [42] contains a bifurcation geometry from a CT scan of a healthy volunteer. An eccentric plaque is artificially inserted in the internal branch. Flow is simulated with the CFD-package Fluent for a cardiac cycle of 1 second in steps of 5 ms. An inlet velocity profile is applied at the common carotid artery, which was obtained from a spectral velocity measurement on the volunteer. Furthermore, rigid walls are assumed with no modeling of tissue movement. Swillens et al. also provide a framework (BioMMeda.ugent.be), where the CFD velocities are used for propagating scatterers and coupled to Field II for ultrasound simulations. Spatial and temporal interpolation are handled by the framework for updating the scatterer positions according to the ultrasound simulation.

B. Flow Rig Measurements

The approach is implemented on the experimental scanner SARUS [33] for acquisition of channel RF data. The setup is the same as for simulations, and a transducer with parameters as listed in Table I is employed. A flow rig system is used, where the radius of the tube is 6 mm. Constant parabolic flow is circulated by a Cole-Parmer centrifugal pump (Vernon Hills, IL, USA), and volume flow is measured by a magnetic flow meter for reference (MAG1100, Danfoss, Nordborg, Denmark). The f_{prf} is reduced to 2 kHz to avoid reverberations in the water tank, and the volume flow in the flow rig system is adjusted to match the peak velocity-to-f_{prf} ratio in the simulations. The match of parameters used in flow rig scans and straight vessel simulations allows for direct comparison between simulations and measurements.

C. In Vivo Measurement

An *in vivo* scan is conducted after approval by the local research ethics committee (Protocol No. H-1-2014-fsp-072). A 27-year old healthy male is scanned after informed consent by an experienced radiologist. The right carotid bifurcation is scanned in a longitudinal view. The scan sequence is the same as for simulation and flow rig measurements, and the f_{prf} is 10 kHz. Data are acquired for 10 s. Discrimination between tissue and blood is based on intensity values in the B-mode images, where intensities below a threshold are considered to be blood.

Intensity and temperature measurements are performed prior to the *in vivo* scan to assure compliance with FDA regulations [43]. Mechanical index (MI) and derated spatial-peak temporal average intensity ($I_{spta.3}$) are measured using the Acoustic Intensity Measurement System AIMS III (Onda Corp., Sunnyvale, CA, USA) and an Onda HGL-0400 hydrophone. The approach described in [44] is used, and results for the sequence are $MI = 1.25$ and $I_{spta.3} = 267$ mW/cm^2. This is within FDA limits, which are $MI = 1.9$ and $I_{spta.3} = 720$ mW/cm^2. Transducer surface temperature rise is measured to 18.6°C in still air and 6.3°C when attached to a phantom. The values are below the FDA limits of 27°C and 10°C, respectively.

IV. Results

A. Simulations

1) Straight vessel phantom: Results for simulated straight vessel phantoms are shown in Fig. 4 and 5 for beam-to-flow angles of 90° and 60°, respectively. The mean velocity magnitude and angles for the center line are shown in black with ±1 SD, and the true velocities and angles are shown in red. Results from the TO estimation are shown in the left

figures, while results for the TO-DB are shown in the right figures. Using TO, the flow angle is accurate especially in the central part of the vessel, and with a larger bias near the vessel walls. Applying TO-DB based on the TO estimates improves the precision of the angle estimates while maintaining a high accuracy. Accuracy and precision of velocity estimates are quantified with mean bias and mean SD relative to the true peak velocity. The velocities are estimated accurately with a bias less than 3% for both TO and TO-DB, and there is a reduction in SD from 5.7% to 1.1% for the 60° beam-to-flow angle when using TO-DB rather than only TO. Relative bias and SD are summarized in Fig. 6 for beam-to-flow angles from 30° to 90°. TO-DB maintains a low SD less than 2° for angles and 2% for velocities at all beam-to-flow angles, while the SD of the TO angle estimate increases significantly, when the beam-to-flow angle is below 60°. There is a small reduction in angle bias using TO-DB rather than only TO, and both TO and TO-DB estimate velocities with a bias less than 4% for all investigated angles. Even though the angles are detected correctly for beam-to-flow angles larger than 60°, there are slightly larger biases on the velocity magnitude estimates for TO-DB than TO. Especially beam-to-flow angles close to 90° are challenging for TO-DB, because the directional (transverse) signals contain mainly low frequencies, and this makes it difficult to accurately detect the lag between the signals.

The variation in SD for TO angles as a function of beam-to-flow angle is also the reason for the choice of different $\Delta\theta$-steps for DB. There is a larger uncertainty in TO angle estimates at smaller beam-to-flow-angles compared to beam-to-flow angles close to 90°. Thus, a larger $\Delta\theta$ is needed to cover 68 % of the estimates for imprecise TO angles. For beam-to-flow angles less than 45°, the SD of the TO angles are 12° - 17°, however, $\Delta\theta$ for DB is set to 10° in (15). The simulations have also been tested for $\Delta\theta = 17°$ at a 30° beam-to-flow angle, but showed no significant improvement in performance compared to $\Delta\theta = 10°$.

Lateral TO velocity estimates, v_x, are obtained after TO filtering prior to applying the phase-shift TO estimator. The filtering removes energy, and the performance of the estimator is therefore investigated for a variation in SNR, see Fig. 7. The performance of the time-shift estimator used for the axial velocity component v_z is also shown in the figure. A loss in SNR degrades the velocity estimates, and the SD of v_x increases significantly when the SNR is below 0 dB, and below 5 dB for v_z. The bias is maintained below 5% for v_z and v_x at 0 dB SNR.

2) CFD simulations: Vector flow images at time instances during peak systole and systolic deceleration are shown in Fig. 8 and 9. The reference CFD frames are shown to the left, where velocity vectors are overlaid on a color wheel map, which depends on both velocity magnitude and angle. The ultrasound simulated estimates after TO and TO-DB processing are shown in the middle and to the right, respectively. There is a good agreement between the reference CFD images and estimated VFI frames as provided by visual inspection of the images. At peak systole in Fig. 8 there are, however, wrong estimations close to the vessel walls, where velocities are low,

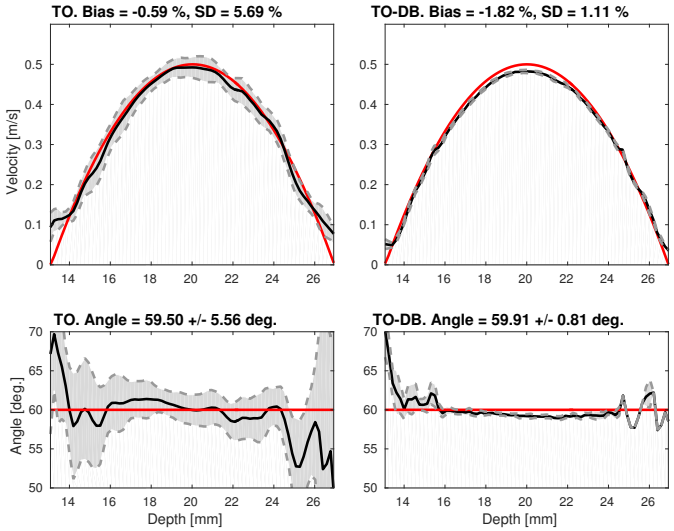

Fig. 5. Simulated velocity profiles for a straight vessel phantom at a 60° beam-to-flow-angle. Velocity magnitude (top) and angles (bottom) for TO (left) and TO-DB (right). Mean estimates are shown in black with ±1 SD and true profiles are in red.

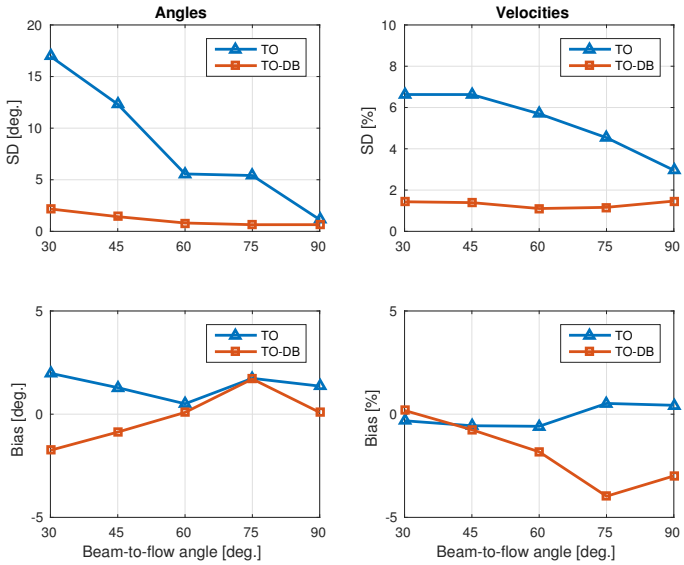

Fig. 6. Results for simulated vessel phantoms with beam-to-flow angles from 30° to 90°. SD (top) and bias (bottom) for estimation of angles (left) and velocities (right). Red graphs show results for TO and blue graphs show results for TO-DB.

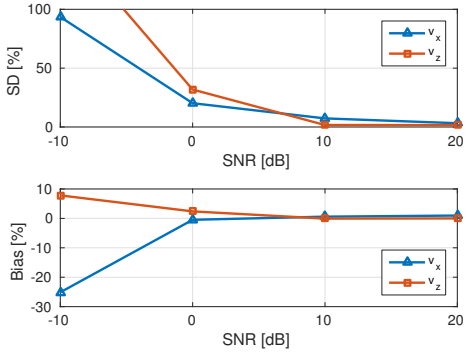

Fig. 7. Variation in SD (top) and bias (bottom) as a function of SNR. Blue graphs are for lateral velocity estimates v_x, and red graphs are for axial velocity estimates v_z.

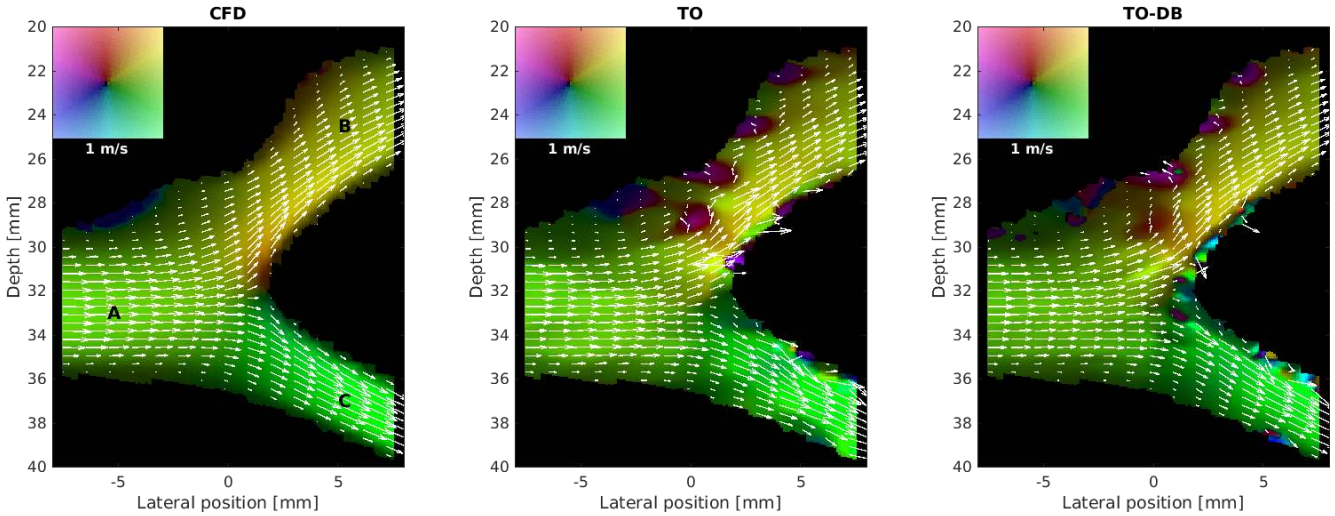

Fig. 8. Results from simulation of flow in a carotid bifurcation model. Frames are shown at peak systole from the reference CFD model (left), estimated velocities using TO (middle), and estimated velocities using TO-DB (right). A, B and C indicate the common, internal, and external carotid artery, respectively

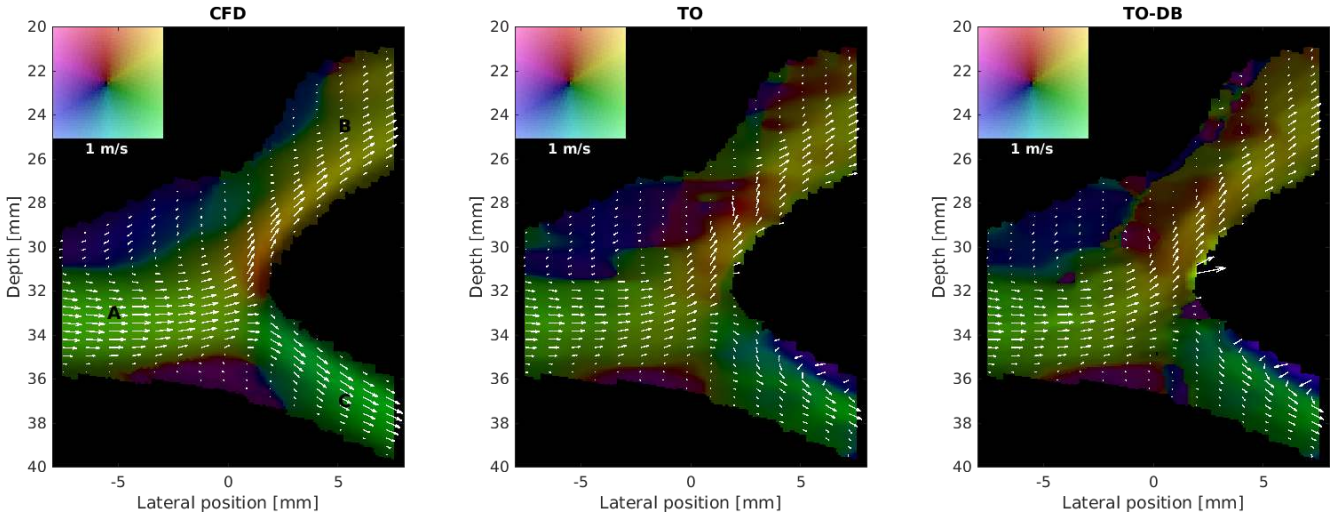

Fig. 9. Results from simulation of flow in a carotid bifurcation model. Frames are shown at systolic deceleration from the reference CFD model (left), estimated velocities using TO (middle), and estimated velocities using TO-DB (right). A, B and C indicate the common, internal, and external carotid artery, respectively

and also areas with wrong angle estimates in the internal carotid artery. Fig. 9 presents complex flow patterns, and the two vortices are clearly visualized and defined using TO-DB. Wrong TO angle estimates with low velocities in the area around (5, 23) mm in the internal carotid artery are corrected with the TO-DB step.

Scatter plots of estimated versus reference velocities and angles are shown in Fig. 10 and 11 to provide a quantitative comparison. Estimated velocities and angles at all spatial points for the frame at peak systole are used for the scatter plots with TO estimates to the left and TO-DB to the right. The colors encode either estimated angle or velocity magnitude, and the straight red lines are the reference values. For velocity magnitude, there is an underestimation of velocities when using TO-DB, represented by a linear regression slope of 0.85 for TO-DB compared to 0.97 for TO. The spread of estimates along the regression line is quantified as the interquartile range, which is 11.8 cm/s for TO and 7.1 cm/s for TO-DB. For the angle scatter plots in Fig. 11, the linear regression slope is 1.01 for both TO and TO-DB, while the angle spread is highest for TO: 6.7° for TO and 4.7° for TO-DB.

It is also seen in Fig. 11 that wrongly estimated angles in the internal carotid artery in Fig. 8 are present as 300° angle estimates for true 60° angles. True angles at 120° (in the external carotid) are also wrongly estimated as random angles. Furthermore, backflow near the upper wall in the common carotid artery (true 240° angles) are estimated as angles ranging from 100° to 200°. The angle errors are further investigated by plotting the distribution of angle errors as a function of velocity as shown in Fig. 12 for TO-DB estimates. It shows that the largest angle errors are found for true velocities less than 0.3 m/s, which are found close to the vessel walls. The angle error is smaller for high velocities.

B. Flow Rig Measurements

Results from flow rig measurements are shown in Fig. 13 for a 90° beam-to-flow angle and in Fig. 14 for a 60°

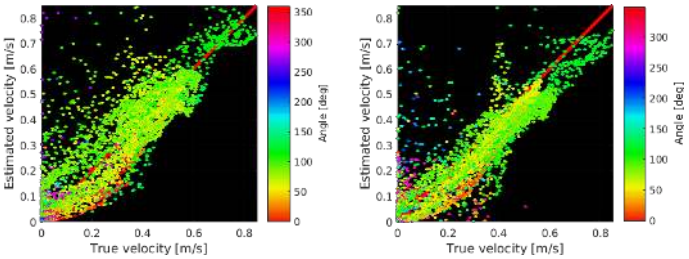

Fig. 10. Scatter plots of true (CFD) velocities versus ultrasound estimations of velocity magnitudes at peak systole. Estimates from TO (left) and TO-DB (right) color encoded with estimated angle.

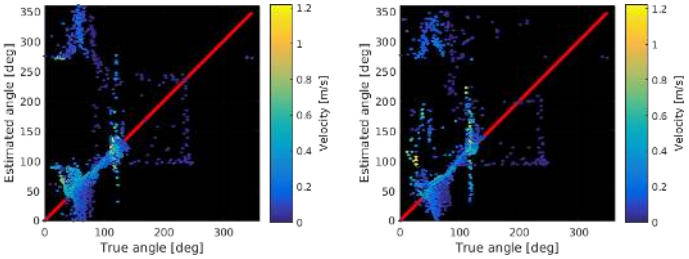

Fig. 11. Scatter plots of true (CFD) angles versus ultrasound estimations of angles at peak systole. Estimates from TO (left) and TO-DB (right) color encoded with estimated velocity.

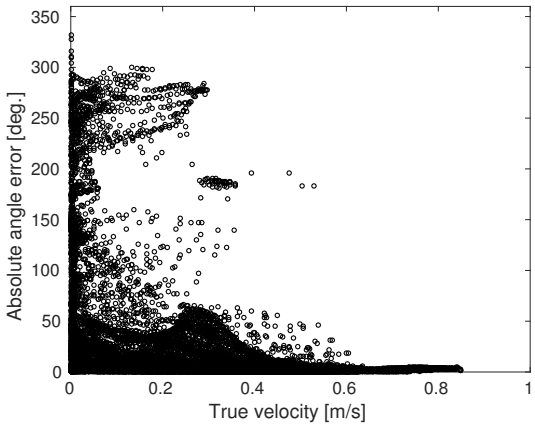

Fig. 12. Scatter plot of the angle error versus velocity magnitude for TO-DB estimation.

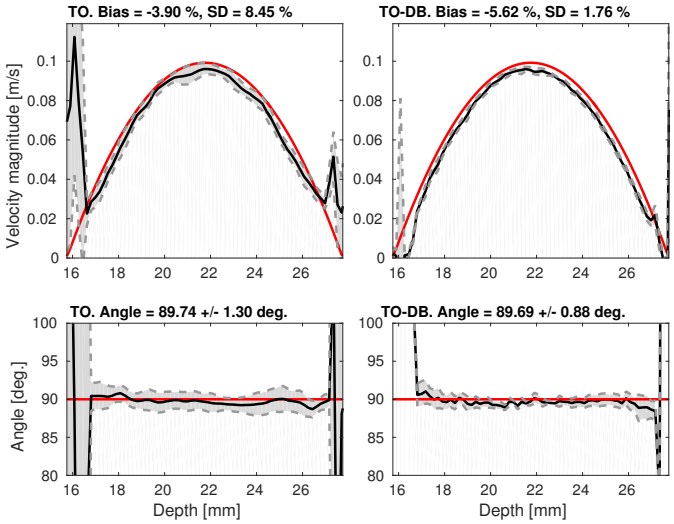

Fig. 13. Measured velocity profiles for a straight vessel phantom at a 90° beam-to-flow-angle. Velocity magnitude (top) and angles (bottom) for TO (left) and DB (right). Mean estimates are shown in black with ±1 SD and true profiles are in red.

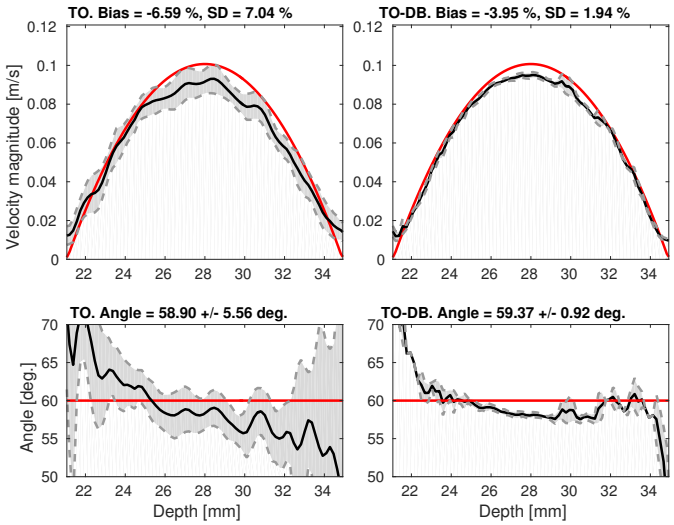

Fig. 14. Measured velocity profiles for a straight vessel phantom at a 60° beam-to-flow-angle. Velocity magnitude (top) and angles (bottom) for TO (left) and DB (right). Mean estimates are shown in black with ±1 SD and true profiles are in red.

beam-to-flow angle. The same trends from the straight vessel simulations are present: a reduction in SD of velocity and angle estimates when using TO-DB rather than only TO, and bias at the same or slightly increased level for TO-DB compared to TO. The wrong estimations close to the vessel walls are due to the echo-canceling filter, which removes all energy from blood and tissue. To avoid the boundary effects, bias and SD are calculated within 90% of the vessel radius. The SD of the velocity magnitude estimates is above 7% when using TO in the two measurements, but is reduced to less than 2% using TO-DB. The 60° beam-to-flow angle is estimated to a mean angle ±1 SD of 58.9°±5.6° using TO and 59.4°±0.9° using TO-DB. The experimental results are overall in good agreement with simulation results, only with a small increase in bias and SD for experiments compared to simulations.

C. In Vivo Measurement

Frames from the *in vivo* scan at peak systole and late systole are shown in Fig. 15, which are processed using TO (left images) and TO-DB (right images). The carotid bifurcation was scanned with a longitudinal view, and the internal carotid is the shallow vessel, while the external carotid is the deep vessel. The direction of flow is indicated by arrows, and reveal a vortex at peak systole in the internal carotid artery. Both TO and TO-DB visualize the vortex, and the TO-DB method estimates a more streamlined flow with less angle spread at the inlet of the internal carotid. TO and TO-DB estimate similar angles and velocities during late systole, however, back-flow close to the vessel walls as estimated using TO is not detected using TO-DB. Low velocities close to vessel walls are challenging to estimate, and since the TO flow angle might

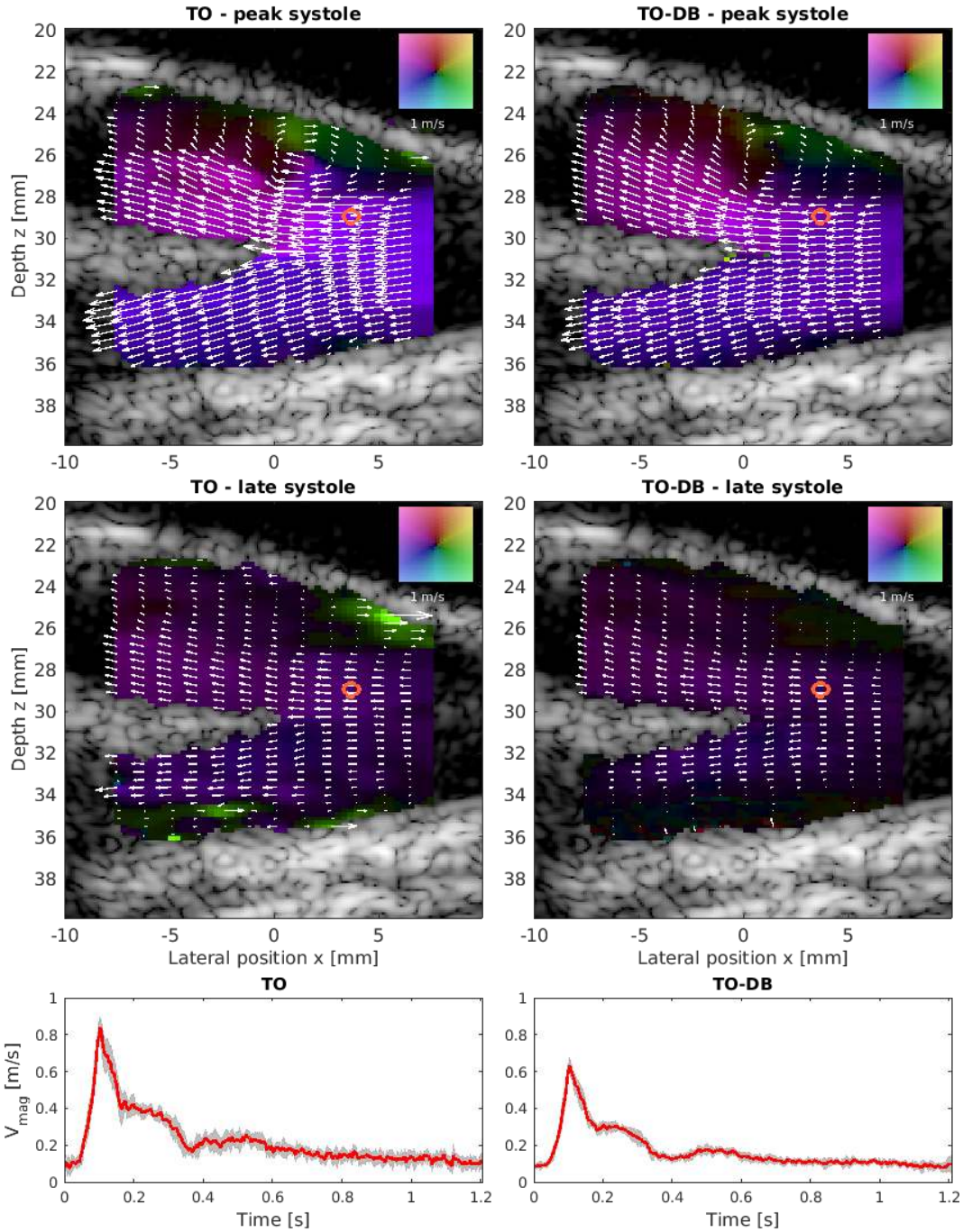

Fig. 15. *In vivo* scan of the carotid bifurcation on a 27 year old healthy volunteer. VFI for frames at peak systole (top) and late systole (middle), and estimates using TO are in the left images while estimates using DB are in the right images. The bottom figures show velocity magnitude at a single estimation point (orange circle on VFI) after alignment to the cardiac cycle. The mean $\pm$ one SD is shown for TO (left) and TO-DB (right).

be estimated wrongly here, the estimated velocity magnitude using TO-DB will be close to zero.

Seven distinct cardiac cycles are detected during the scan acquisition, and the velocity magnitude profiles are divided and aligned to the cardiac cycle. This is shown for the velocity magnitude at the indicated orange circle in Fig. 15 (bottom) for TO (left) and TO-DB (right). The red curves are the mean estimates and the gray area is $\pm$ one SD. The mean SD of the velocity magnitude for TO is calculated to 4.2% and 3.2% for TO-DB. The mean peak velocity is 0.84 m/s for TO and 0.64 m/s for TO-DB. A video sequence from the full acquisition is available as a multimedia attachment, where velocities are estimated at a frame rate of 300 frames/s. This frame rate is fast enough to capture the formation of the vortex present during peak systole, but the frame rate for velocity estimation could be increased to its maximum of 2000 frames/s using the acquired data. The corresponding B-mode imaging has a frame rate of 119 Hz.

Fig. 16 shows a VFI frame at peak systole taken from the same time instance as in Fig. 15 (top). TO is used for velocity estimation, but a Hoeks filter is applied for echo-canceling. The vortex is poorly estimated and flow in the external carotid

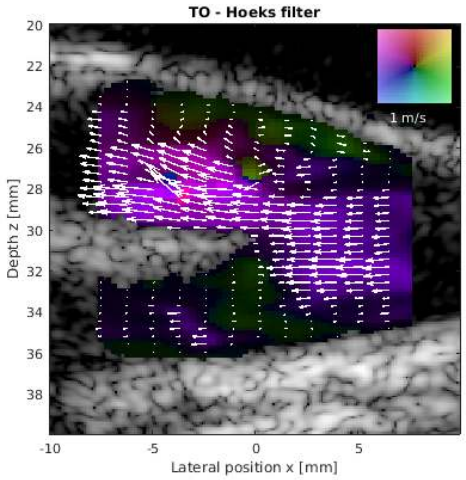

Fig. 16. VFI frame at peak systole using TO for velocity estimation. A Hoeks filter is used for echo-canceling.

artery is lost. Large vessel wall movements and flow in the transverse direction to the ultrasound beam compromise echo-canceling using the Hoeks filter. Low velocities from vessel wall clutter passes the echo-canceling filter and overpowers the blood signal. The example shows that using the energy-based echo-canceling filter is superior to the traditional Hoeks filter in this case.

V. Discussion

The TO-DB method estimates flow angle and velocity magnitude accurately for constant flow in a vessel at all investigated beam-to-flow angles as shown in Fig. 6. The method features a constant low SD less than 2% for velocities and 2° for angles. This is also an improvement compared to TO, which has a SD larger than 6% on the velocity magnitude for small beam-to-flow angles. The bias is within 2% for TO, which is also the case for TO-DB except at 75° and 90°, where bias is closer to 4%. This is still within acceptable levels. An alternative is to compensate for the velocity bias at beam-to-flow angles close to 90°, due to the low bias on the angles and the low SD of both velocity magnitudes and angles. There is also some over and underestimation of the flow angle near the vessel walls (Fig. 5 and 14), which may be due to the echo-canceler, which removes nearly all energy from blood here. The simulation of flow in a bifurcation model provided good estimation of velocities and angles during systolic deceleration, when using TO-DB. Velocities were underestimated during systole (regression coefficient of 0.85 for TO-DB and 0.97 for TO), but with less spread of the estimates for TO-DB. The problem of underestimated velocities around 90° may be solved by increasing the high frequency content in the directional signals, which helps to detect more accurately the lag between signals. It can be achieved by using a lower receive $F\#$ and/or larger steering of the emitted plane waves. The low frequency signals are mainly an issue for broad band estimators like TO-DB, while TO uses a narrow band estimator and mainly considers the phase-shift around a desired lateral oscillation frequency. TO and DB use fundamentally different estimators: TO estimates the velocity vector by two independent axial and lateral estimators, while DB estimates velocity magnitude from a given flow angle. Any small angle error results in underestimated velocities for DB due to the cosine factor.

The initial estimation of angle and velocity using TO can potentially be employed as prior information for TO-DB to choose line length, correlation time, and angle span $\Delta\theta$. Fig. 12 showed that the smallest angle errors were obtained for high velocities, while the angle error increased for low velocities. Estimated velocities scale with f_{prf}, and the angle errors can possibly be reduced for low velocities by reducing f_{prf}. Since continuous data is available, a lower effective f_{prf} can be synthesized artificially during periods with slow flow by skipping HRIs used for velocity estimation, while maintaining the system f_{prf}.

A weakness of the proposed method is its dependence on the TO angle estimate. If the TO angle is estimated with an error more than $\pm\Delta\theta$, then the TO-DB angle estimate will also be biased. The improvement on the angle estimate using TO-DB can only be within the investigated angle span $\pm\Delta\theta$. When the TO-DB angles are detected and the SD of the angle estimates are calculated, it is expected that the SD of the angle estimate will be lower than the angle span, because it limits the search span for angles. Yet, it is not guaranteed that the SD of the velocity magnitude estimate is reduced compared to TO, and that it is detected accurately. This is, however, what is achieved using the method as shown in Fig. 6. It should be noted that other angle spans (15) may be used, or additional lines within the three lines can be beamformed to reduce the angle span, e.g. for small beam-to-flow angles, where the SD of the TO estimates is larger than 10°. It might also reduce the risk of detecting false angles, which would otherwise draw the TO-DB angle away from a correct TO angle. Another proposal could be to use only the TO angle and directionally beamform a line in this direction to estimate velocity magnitude using cross-correlation.

Given a beamforming load for the TO-DB method, which is 4.6 times larger than for TO and seven times smaller than for NCF DB, the method places itself between TO and NCF DB. An exact comparison depends on the implementation details, since optimization can be performed and some beamformed points can be used for several velocity estimation points.

Phase-based velocity estimators for axial and lateral velocity estimation using TO can suffer from aliasing, which limits the maximum detectable velocity. This is especially an issue in SA systems, where the summation of a number of LRIs reduces the effective f_{prf}. However, the lateral wavelength λ_x can be chosen relatively independent. A small value of λ_x can increase the precision for low velocities, while a larger λ_x avoids aliasing for large velocities. If, e.g. $\lambda_x = 0.2$ cm, the maximum v_x is:

$$v_{x,max} = \frac{\lambda_x}{4} f_{prf,eff} = \frac{0.2 \text{ cm}}{4} \cdot 2 \text{ kHz} = 1 \text{ m/s}. \quad (16)$$

This is sufficient for peak velocities during systole and is about four times larger than the maximum detectable v_z ($v_{z,max} = 0.23$ m/s). In this paper, the axial velocity was estimated using

a cross-correlation estimator to circumvent aliasing problems, which may occur for vessels with a beam-to-flow angle less than 75°. The precision of the cross-correlation estimator can, however, decrease for large beam-to-flow angles [32].

The carotid bifurcation scanning on a volunteer demonstrated the feasibility of the method *in vivo*, where tissue movement, absorption, and complex flow patterns complicate vector flow estimation. Peak velocities were estimated lower for TO-DB compared to TO, which was also the case in the simulated bifurcation model. The flow angle is close to 90° at the estimation point, where small angle errors may give an underestimated velocity magnitude. The transmission of a few plane waves per frame (HRI) is a compromise between capturing fast transient flow events, and having HRI with sufficient image quality in terms of contrast and resolution for detailed flow estimation. Plane wave and SA methods also have the advantages of continuous data everywhere in the image, which may improve slow flow estimation [27] and the use of more advanced echo-canceling filters [45].

One must be careful with comparison to other vector flow imaging methods, since different setups can be used and each method has its own strengths and limitations. Reduced performance for the lateral velocity estimate at low beam-to-flow angles were found for phase-based TO [20] and speckle tracking [13], and this trend was confirmed for the TO estimates here. The reduced performance was solved by applying the TO-DB step. On the contrary, cross-beam Doppler methods are susceptible to velocity errors at large beam-to-flow angles [17].

VI. Conclusion

A method for 2-D vector flow imaging where the flow angle is found using a combination of TO and DB was presented. The beamforming load of the TO-DB method is 4.6 times larger than for TO and seven times smaller than for conventional DB. In straight vessel simulations and flow rig measurements, the method estimates flow angle accurately and with a bias and SD less than 2°. The SD of the velocity magnitude estimates is less than 2%, which is 2-3 times less than for the TO method. Simulations of realistic flow in a carotid bifurcation model provided good visualization of complex flow during systolic deceleration when using TO-DB. However, an underestimation of velocities was obtained at peak systole. The method was employed with plane waves in transmit, and this acquisition scheme achieves a very high frame rate of 2000 fps for flow estimation. Such high frame rates can capture fast transient flow events, and it was demonstrated in the carotid bifurcation *in vivo*.

Acknowledgments

This work was supported by grant 82-2012-4 from the Danish National Advanced Technology Foundation and by BK Ultrasound Aps.

References

[1] J. A. Jensen, S. Nikolov, K. L. Gammelmark, and M. H. Pedersen, "Synthetic aperture ultrasound imaging," *Ultrasonics*, vol. 44, pp. e5–e15, 2006.

[2] M. Tanter, J. Bercoff, L. Sandrin, and M. Fink, "Ultrafast compound imaging for 2-D motion vector estimation: application to transient elastography," *IEEE Trans. Ultrason., Ferroelec., Freq. Contr.*, vol. 49, pp. 1363–1374, 2002.

[3] G. E. Trahey, J. W. Allison, and O. T. von Ramm, "Angle independent ultrasonic detection of blood flow," *IEEE Trans. Biomed. Eng.*, vol. BME-34, no. 12, pp. 965–967, 1987.

[4] B. Dunmire, K. W. Beach, K.-H. Labs., M. Plett, and D. E. Strandness, "Cross-beam vector Doppler ultrasound for angle independent velocity measurements," *Ultrasound Med. Biol.*, vol. 26, pp. 1213–1235, 2000.

[5] J. A. Jensen and P. Munk, "A new method for estimation of velocity vectors," *IEEE Trans. Ultrason., Ferroelec., Freq. Contr.*, vol. 45, no. 3, pp. 837–851, 1998.

[6] M. E. Anderson, "Multi-dimensional velocity estimation with ultrasound using spatial quadrature," *IEEE Trans. Ultrason., Ferroelec., Freq. Contr.*, vol. 45, pp. 852–861, 1998.

[7] H. Liebgott, J. Wilhjelm, J. A. Jensen, D. Vray, and P. Delachartre, "PSF dedicated to estimation of displacement vectors for tissue elasticity imaging with ultrasound," *IEEE Trans. Ultrason., Ferroelec., Freq. Contr.*, vol. 54, no. 4, pp. 746–756, 2007.

[8] J. A. Jensen, "Directional velocity estimation using focusing along the flow direction: I: Theory and simulation," *IEEE Trans. Ultrason., Ferroelec., Freq. Contr.*, vol. 50, pp. 857–872, 2003.

[9] S. Ohtsuki and M. Tanaka, "The flow velocity distribution from the doppler information on a plane in three-dimensional flow," *J. of Visualization*, vol. 9, no. 1, pp. 69–82, 2006.

[10] D. Garcia, J. C. del Alamo, D. Tanne, R. Yotti, C. Cortina, E. Bertrand, J. C. Antoranz, E. Perez-David, R. Rieu, F. Fernandez-Aviles, and J. Bermejo, "Two-dimensional intraventricular flow mapping by digital processing conventional color-doppler echocardiography images," *IEEE Trans. Med. Imag.*, vol. 29, no. 10, pp. 1701–1713, 2010.

[11] S. I. Nikolov and J. A. Jensen, "Velocity estimation using synthetic aperture imaging," in *Proc. IEEE Ultrason. Symp.*, 2001, pp. 1409–1412.

[12] ——, "In-vivo synthetic aperture flow imaging in medical ultrasound," *IEEE Trans. Ultrason., Ferroelec., Freq. Contr.*, vol. 50, no. 7, pp. 848–856, 2003.

[13] J. Udesen, F. Gran, K. L. Hansen, J. A. Jensen, C. Thomsen, and M. B. Nielsen, "High frame-rate blood vector velocity imaging using plane waves: simulations and preliminary experiments," *IEEE Trans. Ultrason., Ferroelec., Freq. Contr.*, vol. 55, no. 8, pp. 1729–1743, 2008.

[14] K. L. Hansen, J. Udesen, F. Gran, J. A. Jensen, and M. B. Nielsen, "In-vivo examples of flow patterns with the fast vector velocity ultrasound method," *Ultraschall in Med.*, vol. 30, pp. 471–476, 2009.

[15] J. Bercoff, G. Montaldo, T. Loupas, D. Savery, F. Meziere, M. Fink, and M. Tanter, "Ultrafast compound Doppler imaging: providing full blood flow characterization," *IEEE Trans. Ultrason., Ferroelec., Freq. Contr.*, vol. 58, no. 1, pp. 134–147, January 2011.

[16] I. K. Ekroll, A. Swillens, P. Segers, T. Dahl, H. Torp, and L. Lovstakken, "Simultaneous quantification of flow and tissue velocities based on multi-angle plane wave imaging," *IEEE Trans. Ultrason., Ferroelec., Freq. Contr.*, vol. 60, no. 4, pp. 727–738, 2013.

[17] S. Fadnes, I. K. Ekroll, S. A. Nyrnes, H. Torp, and L. Løvstakken, "Robust angle-independent blood velocity estimation based on dual-angle plane wave imaging," *IEEE Trans. Ultrason., Ferroelec., Freq. Contr.*, vol. 62, no. 10, pp. 1757–1767, October 2015.

[18] B. Y. Yiu, S. S. Lai, and A. C. Yu, "Vector projectile imaging: time-resolved dynamic visualization of complex flow patterns." *Ultrasound Med. Biol.*, vol. 40, no. 9, pp. 2295–2309, sept 2014.

[19] S. Ricci, L. Bassi, and P. Tortoli, "Real-time vector velocity assessment through multigate Doppler and plane waves," *IEEE Trans. Ultrason., Ferroelec., Freq. Contr.*, vol. 61, no. 2, pp. 314–324, 2014.

[20] M. Lenge, A. Ramalli, P. Tortoli, C. Cachard, and H. Liebgott, "Plane-wave transverse oscillation for high-frame-rate 2-D vector flow imaging," *IEEE Trans. Ultrason., Ferroelec., Freq. Contr.*, vol. 62, no. 12, pp. 2126–2137, December 2015.

[21] J. A. Jensen, "Directional transverse oscillation vector flow estimation," *IEEE Trans. Ultrason., Ferroelec., Freq. Contr.*, vol. 63, p. Submitted, 2016.

[22] ——, "Comparison of vector velocity imaging using directional beamforming and transverse oscillation for a convex array transducer," in *Proc. SPIE Med. Imag.*, vol. 9040, 2014, pp. 904 012–1–8.

[23] J. A. Jensen and N. Oddershede, "Estimation of velocity vectors in synthetic aperture ultrasound imaging," *IEEE Trans. Med. Imag.*, vol. 25, pp. 1637–1644, 2006.

[24] C. A. Villagomez-Hoyos, M. B. Stuart, K. L. Hansen, M. B. Nielsen, and J. A. Jensen, "Accurate angle estimator for high frame rate 2-D

vector flow imaging," *IEEE Trans. Ultrason., Ferroelec., Freq. Contr.*, vol. 63, no. 6, pp. 842–853, 2016.

[25] J. Jensen, M. B. Stuart, and J. A. Jensen, "High frame rate vector velocity estimation using plane waves and transverse oscillation," in *Proc. IEEE Ultrason. Symp.*, 2015, pp. 1–4.

[26] J. Jensen, C. A. Villagomez-Hoyos, M. B. Stuart, C. Ewertsen, M. B. Nielsen, and J. A. Jensen, "In vivo high frame rate vector flow imaging using plane waves and directional beamforming," in *Proc. IEEE Ultrason. Symp.*, 2016, pp. 1–4.

[27] E. Mace, G. Montaldo, I. Cohen, M. Baulac, M. Fink, and M. Tanter, "Functional ultrasound imaging of the brain," *Nature methods*, vol. 8, no. 8, pp. 662–664, 2011.

[28] F. Varray and H. Liebgott, "An alternative method to classical beamforming for transverse oscillation images: Application to elastography," *IEEE 10th Int. Symp. Biomedical Imaging*, pp. 716–719, 2013.

[29] S. Salles, A. J. Y. Chee, D. Garcia, A. C. H. Yu, D. Vray, and H. Liebgott, "2-D arterial wall motion imaging using ultrafast ultrasound and transverse oscillations," *IEEE Trans. Ultrason., Ferroelec., Freq. Contr.*, vol. 62, no. 6, pp. 1047–1058, 2015.

[30] J. A. Jensen, "A new estimator for vector velocity estimation," *IEEE Trans. Ultrason., Ferroelec., Freq. Contr.*, vol. 48, no. 4, pp. 886–894, 2001.

[31] O. Bonnefous and P. Pesqué, "Time domain formulation of pulse-Doppler ultrasound and blood velocity estimation by cross correlation," *Ultrason. Imaging*, vol. 8, pp. 73–85, 1986.

[32] S. G. Foster, P. M. Embree, and W. D. O'Brien, "Flow velocity profile via time-domain correlation: Error analysis and computer simulation," *IEEE Trans. Ultrason., Ferroelec., Freq. Contr.*, vol. 37, pp. 164–175, 1990.

[33] J. A. Jensen, H. Holten-Lund, R. T. Nilsson, M. Hansen, U. D. Larsen, R. P. Domsten, B. G. Tomov, M. B. Stuart, S. I. Nikolov, M. J. Pihl, Y. Du, J. H. Rasmussen, and M. F. Rasmussen, "SARUS: A synthetic aperture real-time ultrasound system," *IEEE Trans. Ultrason., Ferroelec., Freq. Contr.*, vol. 60, no. 9, pp. 1838–1852, 2013.

[34] J. Jensen, M. B. Stuart, and J. A. Jensen, "Optimized plane wave imaging for fast and high-quality ultrasound imaging," *IEEE Trans. Ultrason., Ferroelec., Freq. Contr.*, vol. 63, no. 11, pp. 1922–1934, 2016.

[35] J. M. Hansen, M. C. Hemmsen, and J. A. Jensen, "An object-oriented multi-threaded software beamformation toolbox," in *Proc. SPIE Med. Imag.*, vol. 7968, March 2011, pp. 79 680Y–1–79 680Y–9.

[36] A. P. G. Hoeks, M. Hennerici, and R. S. Reneman, "Spectral composition of Doppler signals," *Ultrasound Med. Biol.*, vol. 17, pp. 751–760, 1991.

[37] C. A. Villagomez-Hoyos, "Synthetic aperture vector flow imaging," Ph.D. dissertation, Technical University of Denmark, 2016. [Online]. Available: http://findit.dtu.dk/en/catalog/2347162876

[38] C. A. Villagomez-Hoyos, M. B. Stuart, T. Bechsgaard, M. B. Nielsen, and J. A. Jensen, "High frame rate synthetic aperture vector flow imaging for transthoracic echocardiography," in *Proc. SPIE Med. Imag.*, 2016.

[39] J. A. Jensen and N. B. Svendsen, "Calculation of pressure fields from arbitrarily shaped, apodized, and excited ultrasound transducers," *IEEE Trans. Ultrason., Ferroelec., Freq. Contr.*, vol. 39, pp. 262–267, 1992.

[40] J. A. Jensen, "Field: A program for simulating ultrasound systems," *Med. Biol. Eng. Comp.*, vol. 10th Nordic-Baltic Conference on Biomedical Imaging, Vol. 4, Supplement 1, Part 1, pp. 351–353, 1996.

[41] ——, "A multi-threaded version of Field II," in *Proc. IEEE Ultrason. Symp.* IEEE, 2014, pp. 2229–2232.

[42] A. Swillens, L. Løvstakken, J. Kips, H. Torp, and P. Segers, "Ultrasound simulation of complex flow velocity fields based on computational fluid dynamics," *IEEE Trans. Ultrason., Ferroelec., Freq. Contr.*, vol. 56, no. 3, pp. 546–556, 2009.

[43] FDA, "Information for manufacturers seeking marketing clearance of diagnostic ultrasound systems and transducers," Center for Devices and Radiological Health, United States Food and Drug Administration, Tech. Rep., 2008.

[44] J. A. Jensen, M. F. Rasmussen, M. J. Pihl, S. Holbek, C. A. Villagomez-Hoyos, D. P. Bradway, M. B. Stuart, and B. G. Tomov, "Safety assessment of advanced imaging sequences, I: Measurements," *IEEE Trans. Ultrason., Ferroelec., Freq. Contr.*, vol. 63, no. 1, pp. 110–119, 2016.

[45] C. Demene, T. Deffieux, M. Pernot, B.-F. Osmanski, V. Biran, J.-L. Gennisson, L.-A. Sieu, A. Bergel, S. Franqui, J.-M. Correas, I. Cohen, O. Baud, and M. Tanter, "Spatiotemporal clutter filtering of ultrafast ultrasound data highly increases Doppler and fUltrasound sensitivity," *IEEE Trans. Med. Imag.*, vol. 34, no. 11, pp. 2271–2285, 2015.